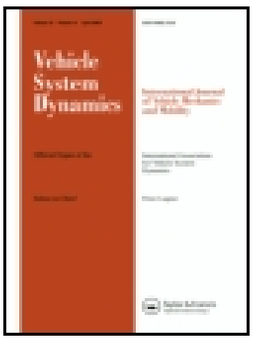

Vehicle System Dynamics

ISSN: 0042-3114 (Print) 1744-5159 (Online) Journal homepage: https://www.tandfonline.com/loi/nvsd20

Improved Vehicle Performance Using Combined Suspension and Braking Forces

ANDREW ALLEYNE

To cite this article: ANDREW ALLEYNE (1997) Improved Vehicle Performance Using Combined Suspension and Braking Forces, Vehicle System Dynamics, 27:4, 235-265, DOI: 10.1080/00423119708969330

To link to this article: https://doi.org/10.1080/00423119708969330

Published online: 27 Jul 2007.

Vehicle System Dynamics, 27 (1997), pp. 235–265 0042-3114/97/2704-235$12.00

Improved Vehicle Performance Using Combined Suspension and Braking Forces

ANDREW ALLEYNE *

SUMMARY

This work presents a preliminary investigation into the integration of particular subsystems of an automobile's chassis. The specific focus of this research is the integration of Active Suspension components with Anti-Lock braking (ABS) mechanisms. The performance objective for the integrated approach is defined as a reduction in braking distance over just anti-lock brakes. Several models, of varying degrees of complexity, are presented to determine the effect of modeling accuracy on the potential performance improvement. In the most detailed model, a four degree of freedom Half Car vehicle model is developed along with models for a hydraulic Active Suspension and an ABS system. For both subsystems, actuator dynamics are included. The tire-road interface is modeled using the Magic Formula tire model. Individual controllers are developed for the subsystems and a governing algorithm is constructed to coordinate the two controllers. Simulations of the integrated controller and an ABS system, for each system model, demonstrate a significant increase in performance.

1. INTRODUCTION

The past decade has seen large advances in the electronic control of various vehicle chassis components. As the speed to cost ratio of computing has dramatically increased, so have the applications to automotive control. Presently, most of the major vehicle chassis components have some type of controller available to them. Anti-lock Braking (ABS) Systems [14] and Traction Control (TC) Systems [15,18] are now standard in the industry. Additionally, a large amount of work has been done in the area of Active Suspensions [1,2]. To date, there have been some preliminary investigations into the coordination of these systems to generate an integrated approach to the control of Vehicle Dynamics. Steering systems are included in many of these early studies. The fundamental principle underlying these efforts is the coordination of forces at the tire-road interface as shown in Fig. 1. Roppenecker and Wallentowitz [16] outline several available strategies for a systems integration approach. Some of the key points of that work are an emphasis on the use of a single group of sensors and/or actuators for multiple vehicle control approaches, thereby reducing cost or increasing signal reliability. For example, the wheel speed sensors and vehicle speed sensors from ABS and TC

* Department of Mechanical and Industrial Engineering, University of Illinois, Urbana-Champaign, Urbana, IL 61801, USA.

systems could be combined and, additionally, the same actuator hardware could be used for both systems. Another key point by [16] is the use of a single control processor module for control of several subsystems. This, combined with streamlining sensor and actuator use, leads to reduced wiring and manufacturing thereby achieving the same vehicle performance with reduced costs. However, no performance results, either by simulation or analysis, are given in [16]. On the vehicle performance side, Matsumoto et al [11] consider the effects of braking force distribution control on yaw rate and vehicle control. Here they try and coordinate the braking at individual wheels to track a desired yaw rate computed from a driver model. Matsumoto and Tomizuka [12] briefly investigate the combination of braking control with steering inputs for steady state turning involving independent lateral velocity and yaw rate control. Xia and Law [20] consider the combination of steering and braking inputs on Four Wheel Steer (4WS) vehicles. Dreyer et al [6] consider the integration of Semi-Active suspensions with ABS/TC and conclude that improved vehicle braking performance could be achieved. The principal reason for this improvement is the reduction of excessive ABS actuation that would result from the control of vehicle pitch during braking. This would minimize the overall amount of wheel slippage thereby lowering the total braking distance. As such, their approach was mostly one of body leveling by appropriate pitch damping.

As is evident, most of the previous research has focused on the coordination of the lateral and longitudinal forces in Fig. 1. The concept of integrating an Active Suspension (vertical forces) with an ABS system (longitudinal forces) has not yet been investigated. This paper will outline an initial study on the coordination of these two systems. The goal is to reduce the vehicle braking distance relative to a system equipped solely with an ABS system. Obviously, the resultant braking will also be superior to that of a passive vehicle without ABS. The reduction in braking distance is achieved by increasing the normal force at the tire-road interface in coordination with the application of the ABS. The Active Suspension will be the tool used to achieve the regulation of the normal force. As mentioned before, others (Dreyer et al. [6]) have examined the use of coordinating the longitudinal aspects of vehicle control (ABS) with vertical control systems (electronic damping). However, most of these systems try to control the gross body motion and

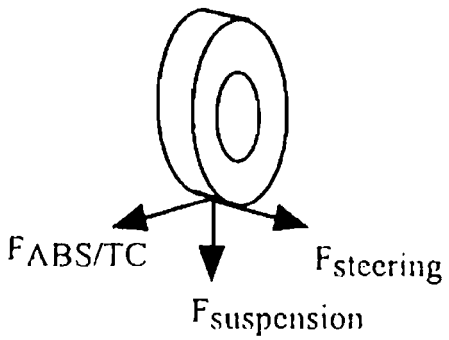

Fig. 1. Tire-road interface forces.

minimize the variation in normal force at the tire-road interface through the minimization of pitch oscillation. This is fundamentally different from the approach to be taken here in which the normal force is modulated in a controlled fashion.

The rest of the paper is organized as follows. Section 2 introduces the basic idea of the coordination of the ABS and active suspension on a two degree of freedom Half Car model and the ABS model. Section 2 also presents the controller for the ABS system and then applies a coordination algorithm for the two inputs assuming that the Active Suspension is a controllable force output. Section 3 includes the dynamics of the unsprung masses to determine the effect of tire natural frequency on the integrated control approach. Section 4 includes the dynamics of the hydraulic actuation system that would be used in such an application and develops a controller for these dynamics. In sections 2, 3, and 4, comparisons will be made between the integrated approach and a standards ABS scheme. A conclusion summarizes the main points of the paper.

2. BASIC CONCEPTS

2.1. Half Car Model

Since the focus of this investigation is vehicle braking performance, the lateral dynamics of the vehicle will be ignored. Consequently, only the longitudinal dynamics will be considered in the vehicle model. Therefore, an adequate model for this system is shown in Fig. 2 below [19].

Using the subscripts f and r to denote the front and rear, define the dynamics of Fig. 2 as:

x: vehicle C.G. forward position
z: vehicle C.G. vertical position
Ip: vehicle pitch inertia about C.G.
q: vehicle pitch angle about C.G.
h: height of C.G. from road
zr: road displacement (= 0 for all t > 0)
zs: sprung mass displacement. from equilibrium

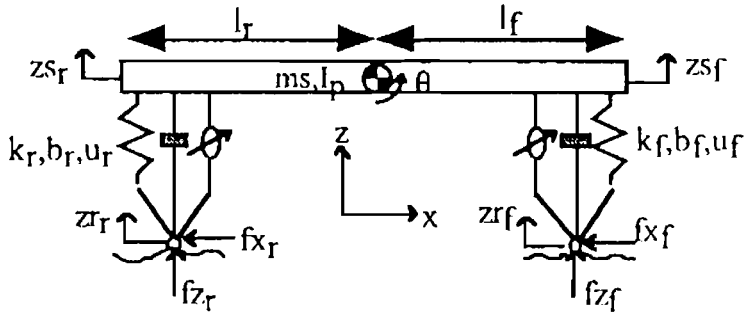

Fig. 2. Half car model.

k: suspension spring constant
b: suspension damping constant
u: active force element
lf: distance from C.G. to vehicle front wheel
lr: distance from C.G. to vehicle rear wheel

Using the above definitions, the dynamics of the Half Car Model can be represented by the following equations

$$\begin{aligned} m_s\ddot{x} &= -fx_f - fx_r \\ m_s\ddot{z} &= f_f + f_r \\ I_p\ddot{\theta} &= f_f l_f - f_r l_r - fx_f(zs_f - zr_f + h) - fx_r(zs_r - zr_r + h), \end{aligned} \tag{2.1}$$

where the suspension forces are defined as

$$\begin{aligned} f_f &= -ks_f(zs_f - zr_f) - bs_f(\dot{z}s_f - \dot{z}r_f) + u_f. \\ f_r &= -ks_r(zs_r - zr_r) - bs_r(\dot{z}s_r - \dot{z}r_r) + u_r. \end{aligned} \tag{2.2}$$

Assuming small angle deflections, the front and rear sprung mass positions are approximated as

$$\begin{aligned} zs_f &= z + l_f\theta. \\ zs_r &= z - l_r\theta. \end{aligned} \tag{2.3}$$

The actuators that provide the suspension input forces, u, in Equation (2.2) are hydraulic pistons controlled by two-stage electro-hydraulic servovalves. However, they will be modeled here as ideal force producing elements.

2.2. Wheel and Tire-Road Interface Models

The model of the ABS system can be developed by considering Fig. 3. Define:
$v = \dot{x}$ = vehicle longitudinal velocity
ω = wheel angular velocity
T_b = brake torque from disks/drums
J = wheel inertia (including any drivetrain effects)
r = effective tire radius.

The equation of motion for the wheel is

$$J\dot{\omega} = \text{Friction Force} \cdot r - T_b. \tag{2.6}$$

The Friction Force (fx) is a function of the wheel slip, λ, which is defined as

$$\lambda = \begin{cases} \dfrac{v - \omega r}{v} & \omega r < v \\ \dfrac{\omega r - v}{\omega r} & \omega r \geq v \end{cases}. \tag{2.7}$$

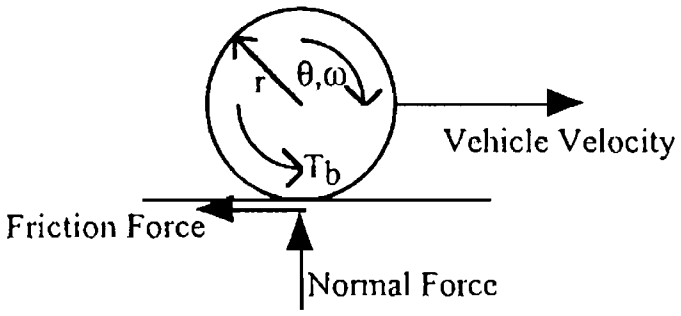

Fig. 3. Wheel coordinates and forces.

In this investigation, vehicle braking is the sole maneuver being considered. Therefore only the first relationship in Equation (2.7) is necessary. The relationship between wheel slip and longitudinal friction force (fx) is usually determined from empirical relationships. Examples of these are the Dugoff Tire Model [7] and the Magic Formula Tire Model [4]. In this analysis, the Magic Formula Tire Model is used. The Magic Formula Tire Model relates longitudinal slip (λ) and normal force (F_z) to longitudinal force (fx) using the compact relationship

$$y(x) = D\sin\left[C\arctan\left\{Bx - E(Bx - \arctan(Bx))\right\}\right], \tag{2.8}$$

with

$$x = \lambda + S_h \quad \text{and} \quad fx(\lambda) = y(x) + S_v.$$

The coefficients in the Magic Formula have a physical meaning with respect to the slip vs. force curve.

B = stiffness factor
C = shape factor
D = peak factor
E = curvature factor
S_h = horizontal shift
S_v = vertical shift

The vertical and horizontal shifts are used to account for offsets in the slip vs. force curves. In this investigation, both shifts will be assumed to be zero. The coefficients above can be influenced by the vertical load on the contact patch at the tire-road interface. Consequently, they can be written as a function of vertical load as follows

$$\begin{aligned} C &= 1.8 \\ D &= a_1F_z^2 + a_2F_z \\ B &= \frac{a_3F_z^2 + a_4F_z}{CDe^{a_5F_z}} \\ E &= a_6F_z^2 + a_7F_z + a_8 \end{aligned} \tag{2.9}$$

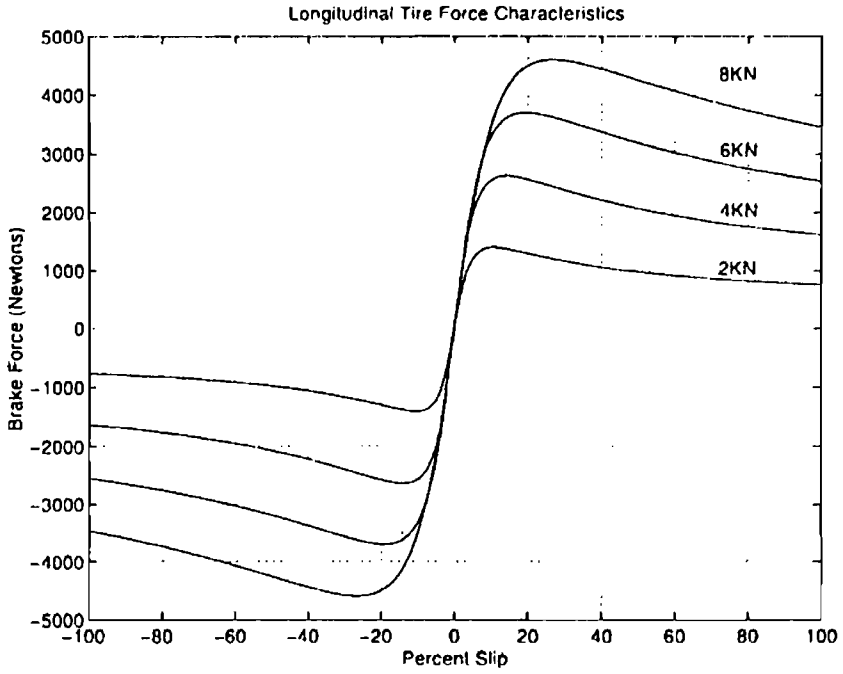

Fig. 4. Magic formula tire model for longitudinal force vs. slip.

A more complete version of the Magic Formula also accounts for camber influences and combined cornering/braking maneuvers. However, for purposes of this analysis, the model given in Equations (2.8) and (2.9) is sufficient. The coefficients that were used in the model and simulations are given as

$$a_1 = -21.3 \quad a_2 = 744.0 \quad a_3 = 49.6 \quad a_4 = 226.0$$
$$a_5 = 0.3 \quad a_6 = -0.006 \quad a_7 = 0.056 \quad a_8 = 0.486$$

The graph of force vs. slip is shown above in Fig. 4. The model of tire force generation given in Fig. 4 corresponds roughly to wet asphalt with a peak friction coefficient of between 0.5 and 0.6. The reader is referred to [8] for additional analysis of 'Force-Slip' curves and ABS systems. The objective of the ABS system is to keep the wheel slip close to the value which generates the peak friction coefficient. This is done by alternately increasing and decreasing the brake torque depending on the value of the wheel slip. A more precise formulation will be given subsequently

2.3. System State Equations

Define the states of the system shown in Fig. 2 to be:

$x_1 = zs_f$ = front suspension deflection $\quad x_2 = \dot{z}s_f$ = front suspension velocity

$x_3 = zs_r$ = rear suspension deflection $\quad x_4 = \dot{z}s_r$ = rear suspension velocity

$x_5 = x$ = vehicle longitudinal position $\quad x_6 = v$ = vehicle longitudinal velocity

$x_7 = \omega_f$ = front wheel angular velocity $\quad x_8 = \omega_r$ = rear wheel angular velocity

The state equations for the system of Fig. 2 can now be written as:

$$\dot{x}_1 = x_2$$

$$\dot{x}_2 = \left(\frac{1}{m_s} + \frac{l_f^2}{I_p}\right) f_f + \left(\frac{1}{m_s} - \frac{l_f l_r}{I_p}\right) f_r - \frac{l_f}{I_p}\left(fx_f(x_1 + h) + fx_r(x_3 + h)\right),$$

with

$$f_f = -ks_f x_1 - bs_f x_2 + u_f.$$
$$f_r = -ks_r x_3 - bs_r x_4 + u_r.$$

$$\dot{x}_3 = x_4$$

$$\dot{x}_4 = \left(\frac{1}{m_s} - \frac{l_f l_r}{I_p}\right) f_f + \left(\frac{1}{m_s} + \frac{l_r^2}{I_p}\right) f_r + \frac{l_r}{I_p}\left(fx_f(x_1 + h) + fx_r(x_3 + h)\right)$$

$$\dot{x}_5 = x_6$$

$$\dot{x}_6 = -\frac{(fx_f + fx_r)}{m_s} \tag{2.10}$$

$$\dot{x}_7 = \frac{1}{J_f}(r_f fx_f - T_{b,f})$$

$$\dot{x}_8 = \frac{1}{J_r}(r_r fx_r - T_{b,r}).$$

2.4. ABS Control Scheme

The inputs to the system in Equation (2.10) are the brake torques ($T_{b,f}$, $T_{b,r}$) and the forces provided by the active suspension actuator (u_f, u_r). At each wheel, the objective for the ABS system modeled here is to keep the wheel slip (λ) close to the peak value (λ_{peak}) on the 'Force-Slip' curve. One control approach to meet this objective is a variable-structure Sliding Mode controller [17]. The goal of the Sliding Mode Controller is to force the dynamics of the system to be constrained to an invariant manifold after some finite time t. A schematic of a 2 dimensional sliding condition is shown in Fig. 5. The arrows in the figure show the evolution of the system state towards the manifold in R^2 regardless of the initial system location in the state space. The controller forces the system dynamics to converge to the surface $S(t) = 0$, which is an m-dimensional manifold where $m < n$ and n is the dimension of the system. This lower dimensional manifold is termed the "Sliding Surface." Once the dynamics of the system reach $S(t) = 0$, the system is constrained to evolve on the $(n - m)$ dimensional space. The key is to choose S(t) such that the properties of the system in the lower dimensional space are desirable.

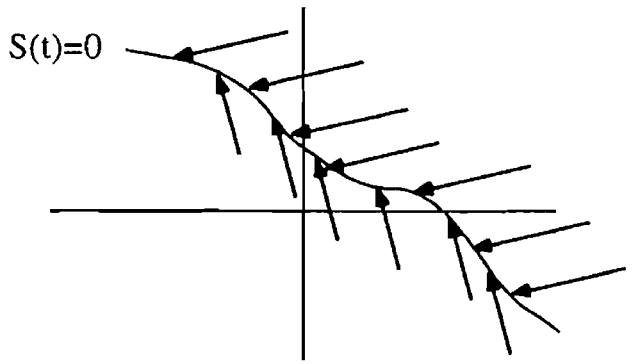

Fig. 5. R^2 sliding condition.

One method to guarantee the convergence of the system to the sliding surface is by designing the control algorithm to ensure that

$$\frac{d}{dt}(S^2(t)) \leq k|S(t)|. \tag{2.11}$$

This leads to a controller with a variable structure to it. The structure of the controller varies with its location in the state space: $S(t) > \text{or} < 0$. A controller similar to this was considered in Tan [18] for an ABS system. A simple, variable structure, Sliding Mode Controller for wheel slip control using brakes is given as follows. If the maximum allowable brake torque is defined as M, the brake torque input to the wheels becomes:

$$T_b = \begin{cases} M \text{ if } \lambda < \lambda_{peak} \\ 0 \text{ if } \lambda > \lambda_{peak} \end{cases} \tag{2.12}$$

Theoretically, if the brake torque could be completely controlled, then the optimal wheel slip could always be maintained. The braking dynamics of the vehicle would then evolve along the sliding manifold defined by $\lambda = \lambda_{peak}$ which would correspond to the highly desirable condition of maximum deceleration. However, this would require infinitely fast switching of the brake torque input about the peak wheel slip value. If this control strategy were to be applied, excessive chattering of the input hardware would result, possibly leading to wear and component failure. A more realistic approach includes the dynamics of the brake actuator which can be modeled as a first order system shown below:

$$\dot{T}_b = \begin{cases} C_{fill}(-T_b + K_b v_b) & \text{fill stage} \\ C_{dump}(-T_b + K_b v_b) & \text{dump stage} \end{cases} \tag{2.13}$$

where C_{fill} and C_{dump} represent the time constants of the brake cylinder's fill and dump phases. Therefore, the brake torque at the front and rear wheels are added as

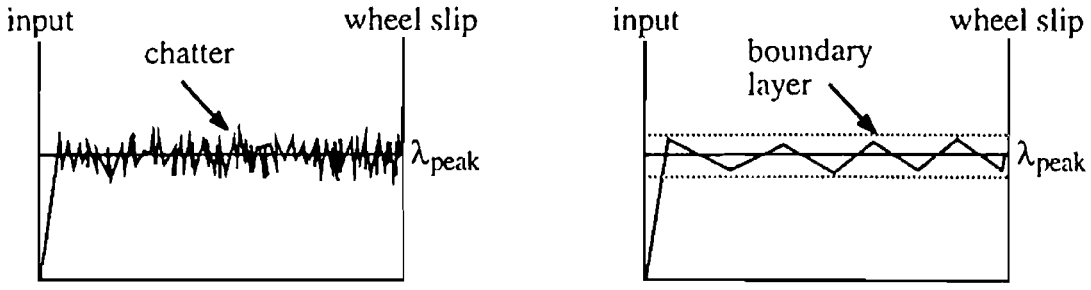

Fig. 6. Variable structure controller without and with boundary layer (schematic).

states to the system equations in (2.10). This model does not include the hold phase of the brake cylinder. v_b is a constant supply pressure that is regulated by an on-off solenoid valve. It is assumed that the dynamics of the valve are much faster than the dump and fill time constants and can therefore be neglected. The brake gain K_b is a function of brake radius, brake pad friction coefficient, brake temperature, and number of pads. K_b converts the brake pressure to brake torque. The control strategy for the ABS system is a simple variable structure controller operating within a boundary layer about the peak wheel slip value.

$$K_b v_b(t) = \begin{cases} M & \forall \lambda < \lambda_{peak} - \dfrac{\varepsilon}{2} \\ 0 & \forall \lambda > \lambda_{peak} + \dfrac{\varepsilon}{2} \\ K_b u_b(t - \Delta t) & \forall |\lambda - \lambda_{peak}| < \dfrac{\varepsilon}{2} \end{cases} \tag{2.14}$$

The boundary layer with magnitude ε is introduced to avoid control chattering about λ_{peak} and Δt is the controller sampling time. Fig. 6 shows the qualitative difference in implementation between control algorithms (2.12) and (2.14).

The coordination of the active suspension and the brake torque input described by Equation (2.14) will be developed and implemented separately at each wheel. Therefore, there will be no coordination between the front and rear wheels. The normal force at each wheel is the sum of the suspension forces and the dynamic weight of the vehicle. The goal of the subsystem integration is to have the normal force on the tire change in phase with the brake torque being applied. When the brake torque is high, the normal force would be high and vice versa. The net effect is a perceived increase in normal tire force with no increase in vehicle inertia. The integration algorithm is represented by

$$F_z = A \cdot \operatorname{sign}\left(T_b - \bar{T}_b\right), \tag{2.15}$$

with $\bar{T}_b$ denoting the mean brake torque on the wheel during braking, F_z denoting the output of the suspension actuator, and A denoting the amplitude of the force

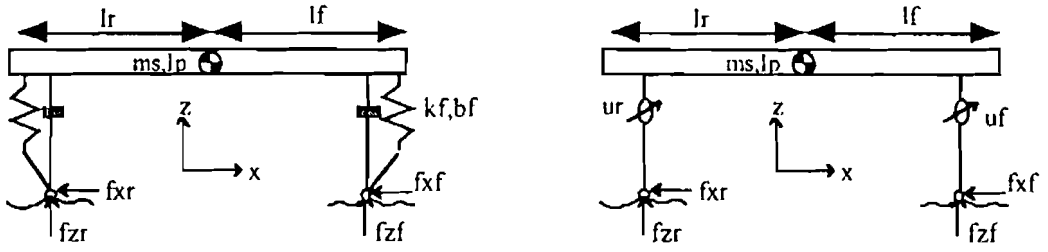

Fig. 7. Half-car models with passive and active suspensions.

desired from the active suspension actuator. It is necessary to have the normal force cycle positive and negative so as to provide an approximate zero mean force to the sprung mass. This will minimize suspension deflection, which will be obviously limited by actuator stroke. The amplitude of the force cannot be made arbitrarily large since it affects the acceleration of the vehicle's sprung mass. Using a Janeway or Burton-Douglas [8] criterion indicates that at approximately 4–5 cycles per second (ABS frequency), the recommended limit of vertical vibration displacement amplitude is on the order of 0.0025 m. Converting this to acceleration, gives a peak acceleration around 0.2 g's ($|accel| = |displ| * 4 * \pi^2 * f^2$). This corresponds to forces on the sprung mass between 500N and 1000N assuming no dynamics (e.g. bushings) between the suspension actuator and the sprung mass. While there have been many studies to correlate vertical vibration to human comfort [8], an extensive study of the maximum permissible value of A would include such variables as human biodynamics, seat transmissibility, steering column transmissibility, etc. Such an investigation is beyond the scope of this presentation. In the following comparisons between ABS and the integrated approach, the effect of A will be examined by numerical simulation.

2.5. Simulations

A simulation comparison will be made between a Half Car system of Fig. 1 with ABS plus a passive suspension versus a vehicle with ABS plus an active suspension. Fig. 7 shows the schematic of the two systems. Fig. 8 shows the schematic of the logic used in the control system of integrated ABS and active

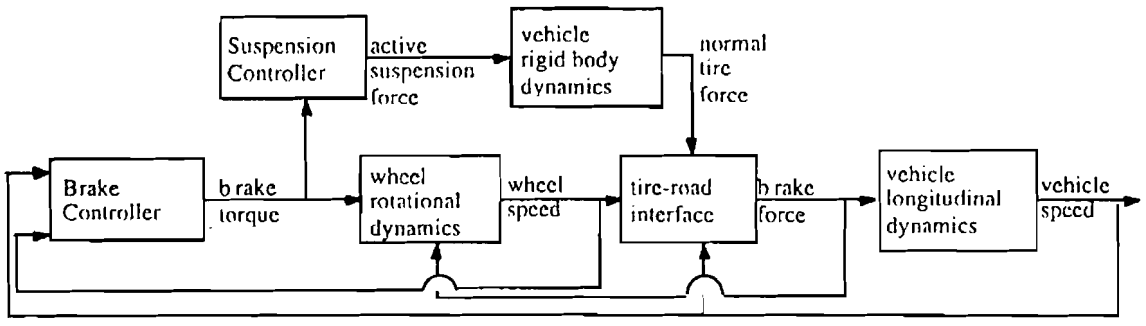

Fig. 8. Control logic diagram.

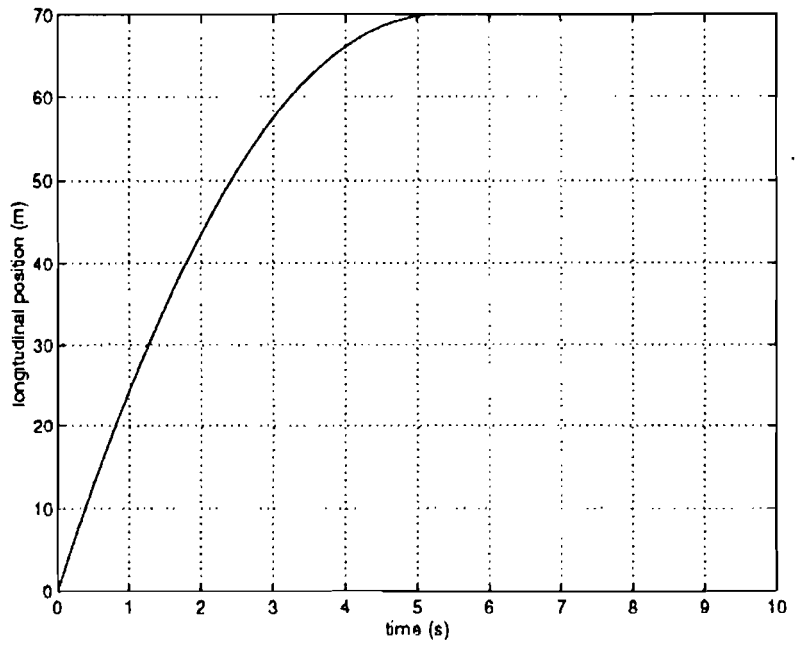

Fig. 9. Vehicle position.

suspension. As can be seen in the figure, the Brake Controller uses the vehicle speed and wheel speed states to determine the wheel slip and, after some dynamics, produce the brake torque state. The Suspension Controller then uses the brake torque state, in an open loop fashion, to determine the appropriate suspension force. The values used in the simulations are given below [1,18,19].

$m_s = 730.0\,kg$	$I_p = 1230.0\,kg - m^2$	$r = 0.3\,m$
$J_f = 1.4\,kg - m^2$	$J_r = 1.0\,kg - m^2$	$ks_f = 19960.0\,N/m$
$ks_r = 17500.0\,N/m$	$bs_f = 1050.0\,N - s/m$	$bs_r = 900.0\,N - s/m$
$l_f = 1.011\,m$	$l_r = 1.803\,m$	$h = 0.508\,m$
$M = 2000\,N - m$	$C_{fill} = 15.0$	$C_{dump} = 15.0$

The initial velocity of the vehicle is 27 m/s or approximately 60 mph. The simulations are carried out in FORTRAN using a 4th order Runge-Kutta integration routine with a fixed time step. Fig. 9 shows the position vs. time of a vehicle using just ABS and Fig. 10 shows the wheel speed for the front wheel only. The data for the rear wheel is similar, with a slightly slower oscillation, and is not shown here. These figures clearly shows the regions of increasing and decreasing wheel slip which correspond to the filling and dumping of the brakes. Fig. 11 shows the brake torque being applied to the front wheel. As with Fig. 10, the data for the rear wheel is similar and is not shown here. Since there is no active suspension force in this case, the variation in normal force on the road is purely a

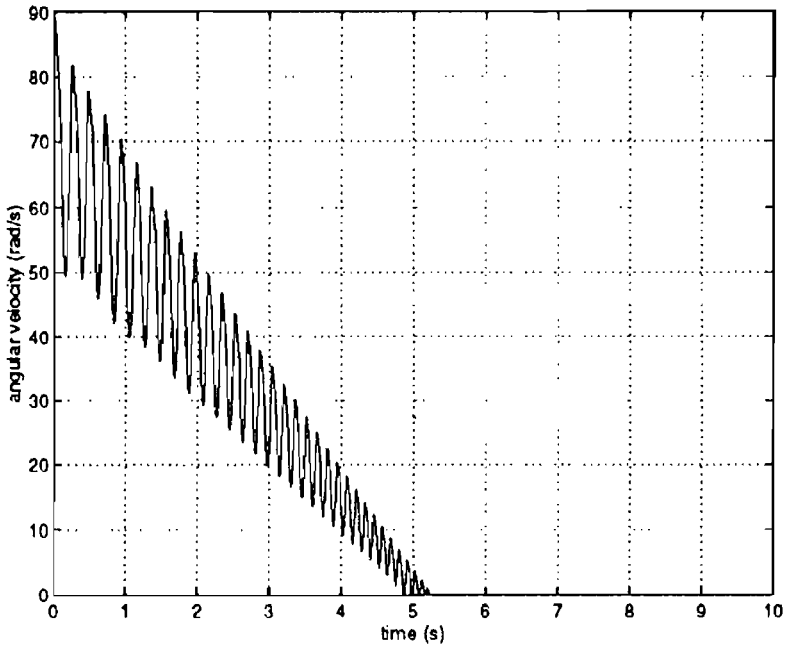

Fig. 10. (ABS) front wheel speed.

function of the dynamic weight transfer. The front tire normal force is shown in Fig. 12. The dynamic weight transfer during braking is from front to rear so the rear tire normal force would be the reflection of Fig. 12 about the equilibrium force ($\sim$ 5000 N) shown at t = 10 seconds. The rear tire normal force is not shown here.

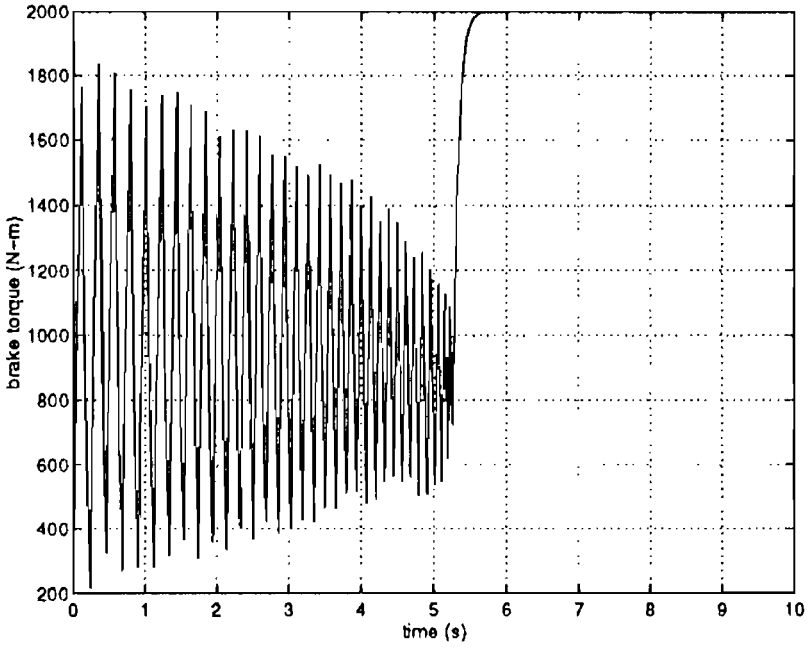

Fig. 11. (ABS) front brake torque.

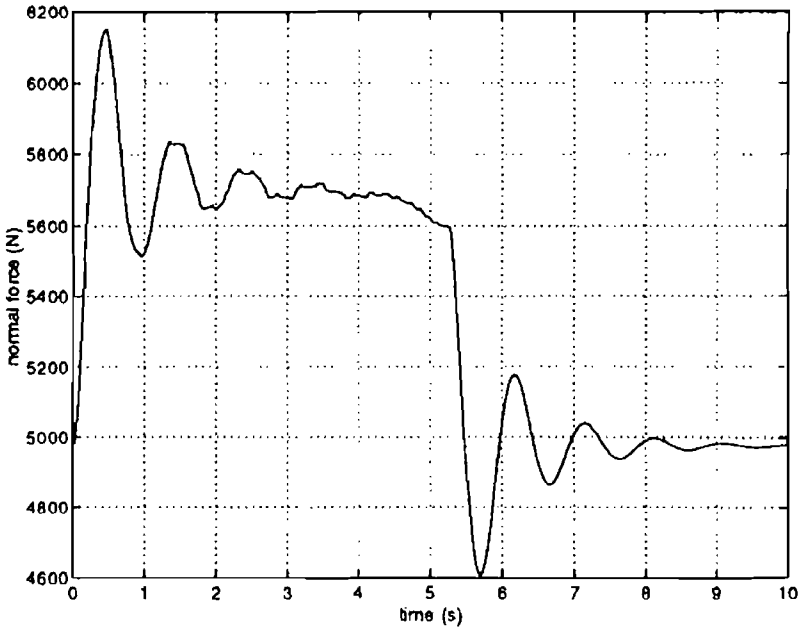

Fig. 12. Front tire normal force.

For comparison, Fig. 13 shows the longitudinal vehicle position with the integrated (ABS and Active Suspension) control approach as well as the passive (ABS only) approach. In the simulation, the amplitude of the desired normal force modulation is given to be 1000 N. The actual force that is applied is the output of a 1st order system with a time constant of 0.03. This was done to give at least some simple dynamics to the suspension actuator as well. Using the integrated approach with a normal force modulation of 1000 N, the braking distance is

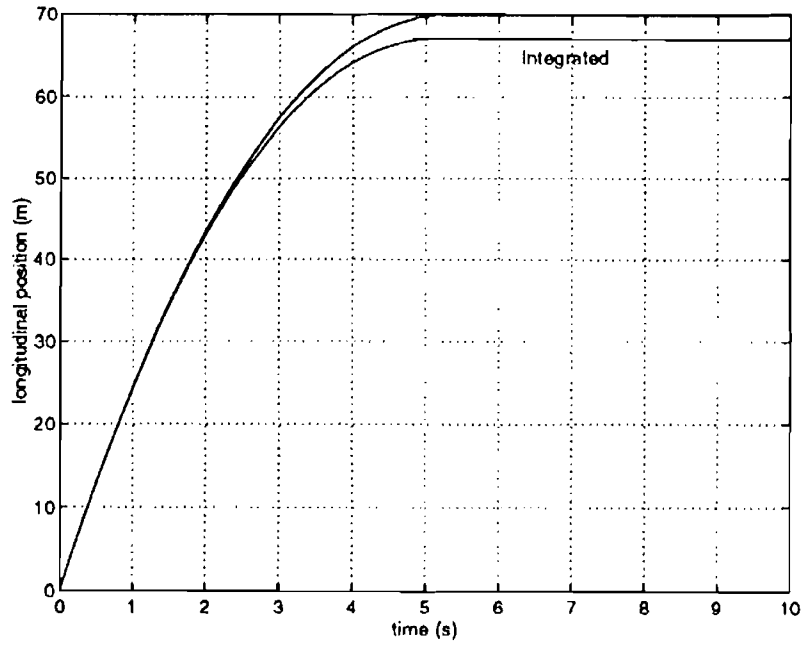

Fig. 13. (Integrated) vehicle position.

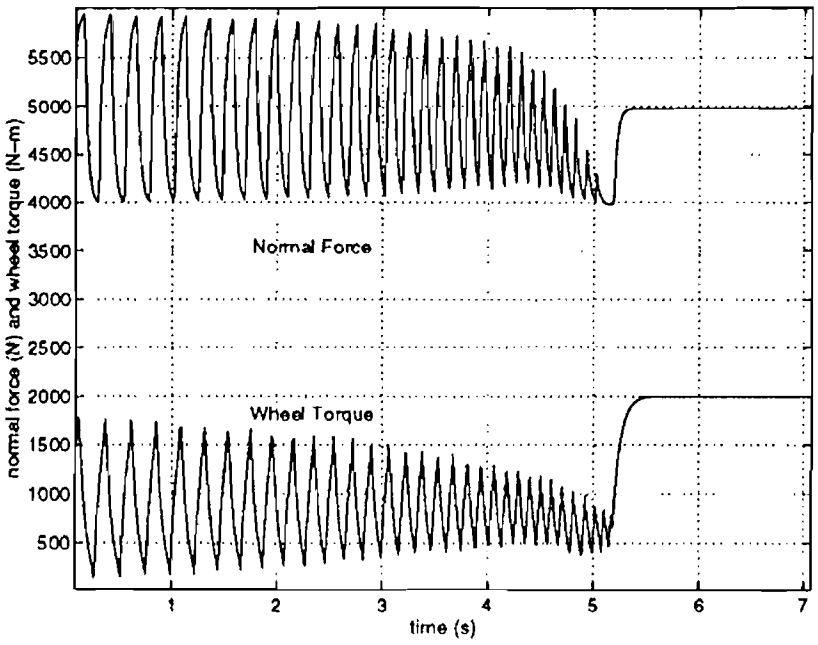

Fig. 14. Brake torque and normal force.

reduced by ~ 4–5% over just ABS. As is seen in Fig. 14, the brake torque and the normal force are in phase which leads to the reduction in stopping distance shown in Fig. 13. The effect of normal force amplitude variation is shown above in Fig. 15. In this figure, three different amplitudes of the normal force cycling are compared: 500 N, 1000 N, 1500 N. As would be expected, an increase in normal force oscillation amplitude will result in a shorter stopping distance. However, the

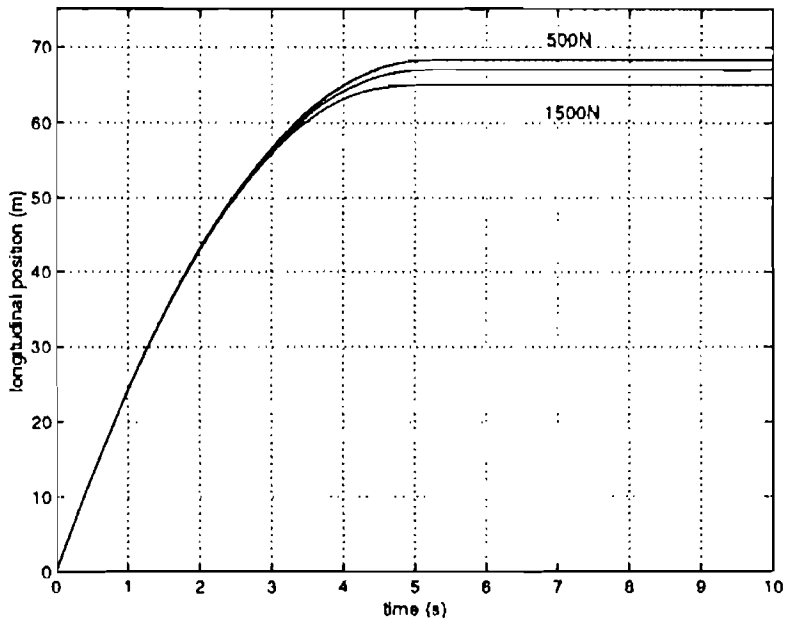

Fig. 15. Stopping distance variation with normal force amplitude.

relationship between the amplitude of the normal force modulation and the stopping distance is not a linear one.

3. MODEL AUGMENTATION: WHEEL VIBRATIONAL MODES

3.1. Half Car Model and State Equations

While the development and simulations of Section 2 introduce the main idea of this work, the results that were given there do not consider wheel dynamics. Since the active suspension element will be cycling the force output at a relatively high frequency, it is possible that such a system may excite the natural frequency of the tires which is typically around 10Hz. For a more valid result, the inclusion of the wheel dynamics is necessary. Fig. 16 shows the augmented system model. The dynamics are similar to Fig. 1 except that the following variables are included:

mu:	unsprung mass	(front = 40 kg,	rear = 35 kg)
kt:	tire spring constant	(front = 175500 N/m,	rear = 175500 N/m)
bt:	tire damping constant	(front = 1500 N/m/s,	rear = 1500 N/m/s)

For vertical oscillations, the tire is treated as a simple spring-damper system based on step response tests conducted at The University of California, Berkeley [5]. In this model the dynamic effects of a rolling tire are not considered. The new dynamics of the unsprung mass are now included to augment the state space description given in Equation (2.10). Redefining the states of the system to be:

$$x_1 = zs_f - zu_f = \text{front suspension deflection}$$
$$x_2 = \dot{z}s_f = \text{front sprung mass velocity}$$
$$x_3 = zu_f - zr_f = \text{front tire deflection}$$
$$x_4 = \dot{z}u_f = \text{front unsprung mass velocity}$$
$$x_5 = zs_r - zu_r = \text{rear suspension deflection}$$
$$x_6 = \dot{z}s_r = \text{rear sprung mass velocity}$$
$$x_7 = zu_r - zr_r = \text{rear tire deflection}$$
$$x_8 = \dot{z}u_r = \text{rear unsprung mass velocity}$$
$$x_9 = x = \text{vehicle longitudinal position}$$
$$x_{10} = v = \text{vehicle longitudinal velocity}$$
$$x_{11} = \omega_f = \text{front wheel angular velocity}$$
$$x_{12} = T_{b,f} = \text{front brake torque}$$
$$x_{13} = \omega_r = \text{rear wheel angular velocity}$$
$$x_{14} = T_{b,r} = \text{rear brake torque}$$

The state equations of Fig. 16 can be written as

$$
\text{rigid body modes}\left\{\begin{aligned}
\dot{x}_1 &= x_2 - x_4\\
\dot{x}_2 &= \left(\frac{1}{m_s} + \frac{l_f^2}{I_p}\right) f_f + \left(\frac{1}{m_s} - \frac{l_f l_r}{I_p}\right) f_r - \frac{l_f}{I_p}\left[fx_f(x_1 + x_3 + h)\right.\\
&\quad \left. + fx_r(x_5 + x_7 + h)\right]\\
&\text{with} \quad f_f = -ks_f x_1 - bs_f(x_2 - x_4) + u_f\\
&\qquad\; f_r = -ks_r x_5 - bs_r(x_6 - x_8) + u_r\\
\dot{x}_3 &= x_4 - \dot{z}r_f\\
\dot{x}_4 &= \frac{1}{mu_f}\left(-f_f - kt_f x_3 - bt_f(x_4 - zr_f)\right)\\
\dot{x}_5 &= x_6 - x_8\\
\dot{x}_6 &= \left(\frac{1}{m_s} - \frac{l_f l_r}{I_p}\right) f_f + \left(\frac{1}{m_s} + \frac{l_r^2}{I_p}\right) f_r + \frac{l_r}{I_p}\left(fx_f(x_1 + x_3 + h)\right.\\
&\quad \left. + fx_r(x_5 + x_7 + h)\right)\\
\dot{x}_7 &= x_8 - \dot{z}r_r\\
\dot{x}_8 &= \frac{1}{mu_r}\left(-f_r - kt_r x_7 - bt_r(x_8 - \dot{z}r_r)\right)
\end{aligned}\right.
$$

$$
\text{vehicle motion}\left\{\begin{aligned}
\dot{x}_9 &= x_{10}\\
\dot{x}_{10} &= -\frac{(fx_f + fx_r)}{ms + mu_f + mu_r}
\end{aligned}\right.
$$

$$
\text{wheel states}\left\{\begin{aligned}
\dot{x}_{11} &= \frac{1}{J_f}(r_f fx_f - x_{12})\\
\dot{x}_{12} &= \tau(-x_{12} + K_{b,f} v_{b,f}) \qquad \tau \in [C_{fill}, C_{dump}]\\
\dot{x}_{13} &= \frac{1}{J_r}(r_r fx_r - x_{14})\\
\dot{x}_{14} &= \tau(-x_{12} + K_{b,r} v_{b,r}) \qquad \tau \in [C_{fill}, C_{dump}]
\end{aligned}\right. \tag{3.1}
$$

3.2. Simulations

As in Section 2, a comparison will be carried out between an ABS equipped vehicle with a passive suspension and one with an Active Suspension. Fig. 17 through 22 show the response for the passive half car. Since the response of the

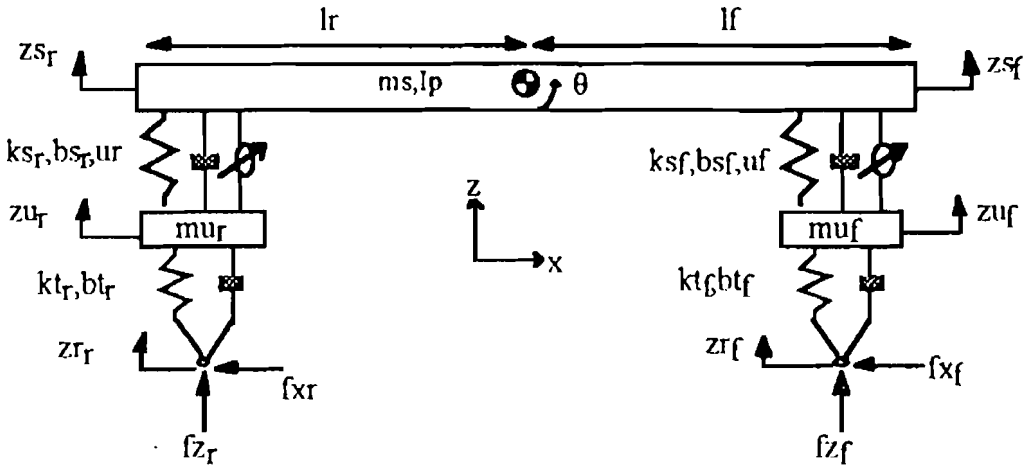

Fig. 16. 4 Degree of freedom half car model.

rear wheel is similar to that of the front, only the response of the front wheel is shown in the figures. Fig. 17 shows the longitudinal position of the passive suspension car and Fig. 18 shows the front wheel speed. Fig. 19 shows the front brake torque and Fig. 20 shows the normal force at the tire road interface. A careful examination of Fig. 20 reveals that the normal force oscillations are not exactly the same as those of Fig. 12 due to the inclusion of the unsprung mass dynamics. The dynamics of the unsprung mass can be seen in Fig. 21 which shows the deflection of the front tire during braking. Since the weight is transferred to the front, the negative tire deflection in Fig. 21 corresponds to a compression of the tire. This is consistent with the definition of the tire deflection state in Equation (3.1). Fig. 22 shows the slip of the front wheel. The wheel slip oscillates between 5 and 45 percent, until the vehicle speed becomes relatively low. At that time, the

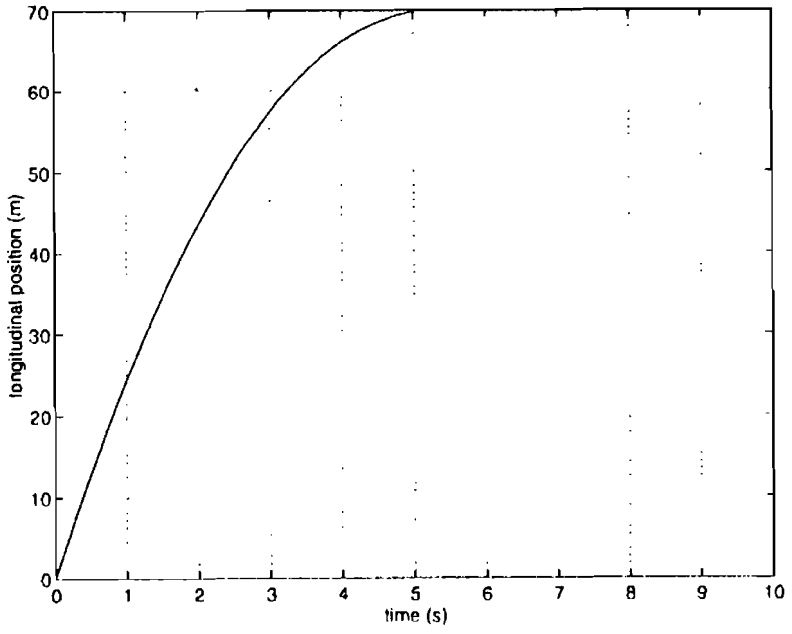

Fig. 17. (ABS) vehicle position.

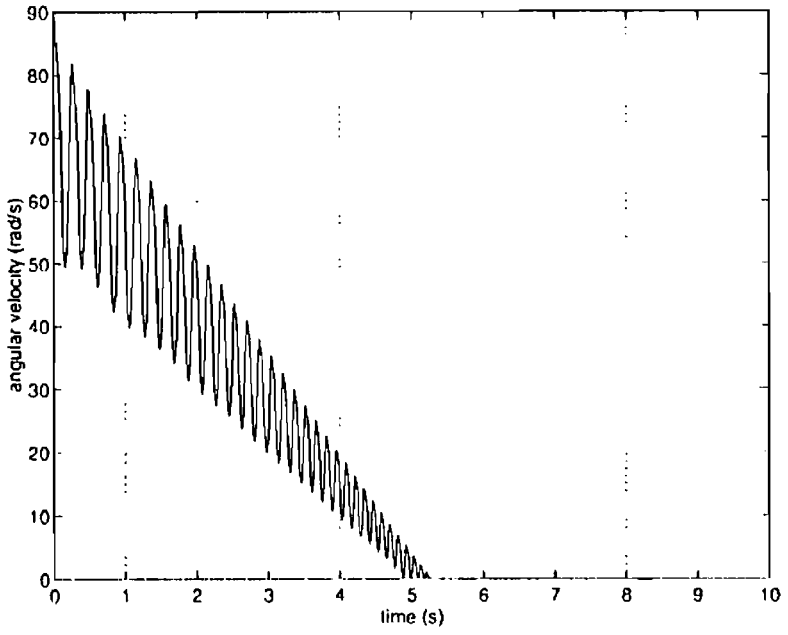

Fig. 18. (ABS) front wheel speed.

slip values increase. This increase is largely a result of the required brake torque oscillation frequency exceeding the bandwidth of the fill and dump time constants in the model. This phenomenon occurs for all of the models in this work. Fig. 23 shows the stopping distance for the integrated system with ABS and Active Suspension. As with the simpler model, there is a significant decrease in the stopping distance ($\sim 5\%$) for the Integrated Chassis Control approach. Even with the effect of the unsprung mass dynamics the integrated approach still is able to

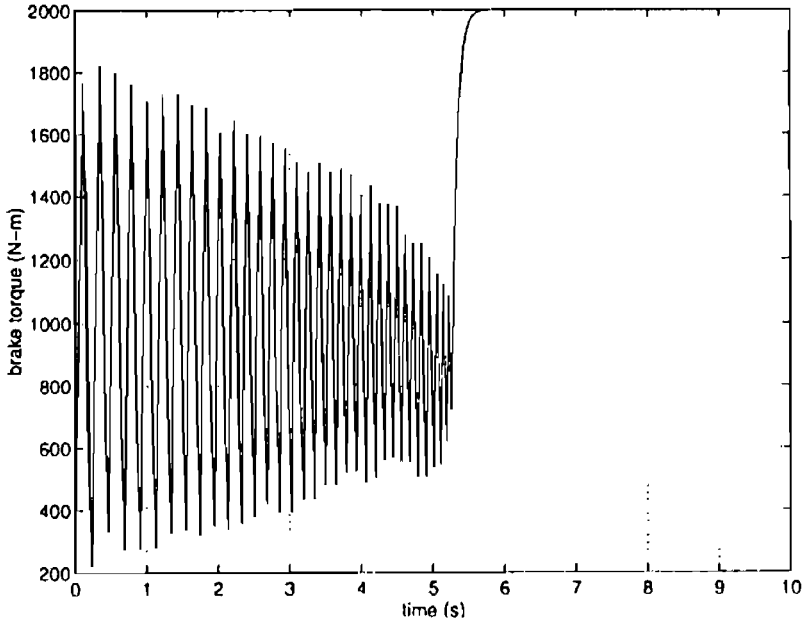

Fig. 19. (ABS) front brake torque.

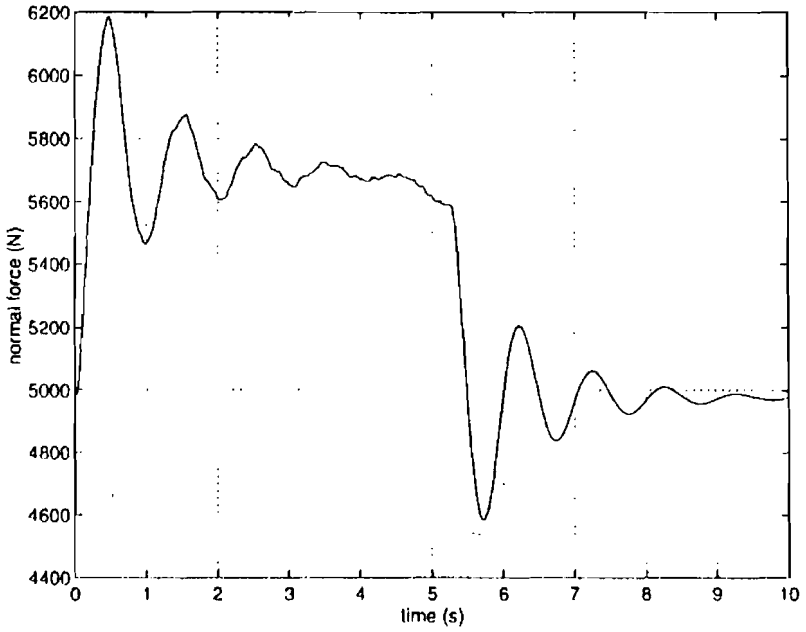

Fig. 20. (ABS) front normal force.

perform well. Fig. 24 shows the coordination of the braking torque and the normal force.

4. MODEL AUGMENTATION: SUSPENSION ACTUATOR DYNAMICS

4.1. Hydraulic Actuator Models

In Sections 2 and 3, the dynamics associated with the Active Suspension force were largely neglected. However, the generation of the desired force is a difficult

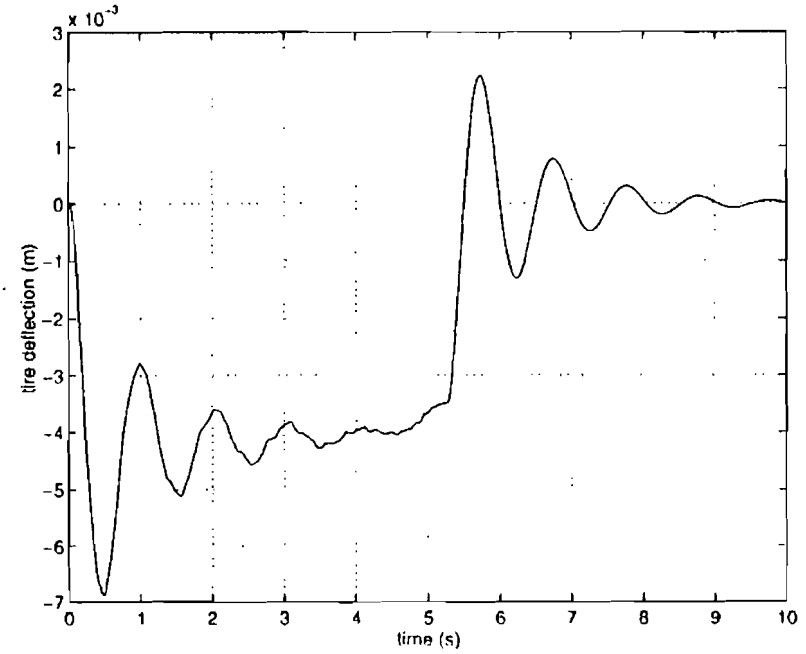

Fig. 21. (ABS) front tire deflection.

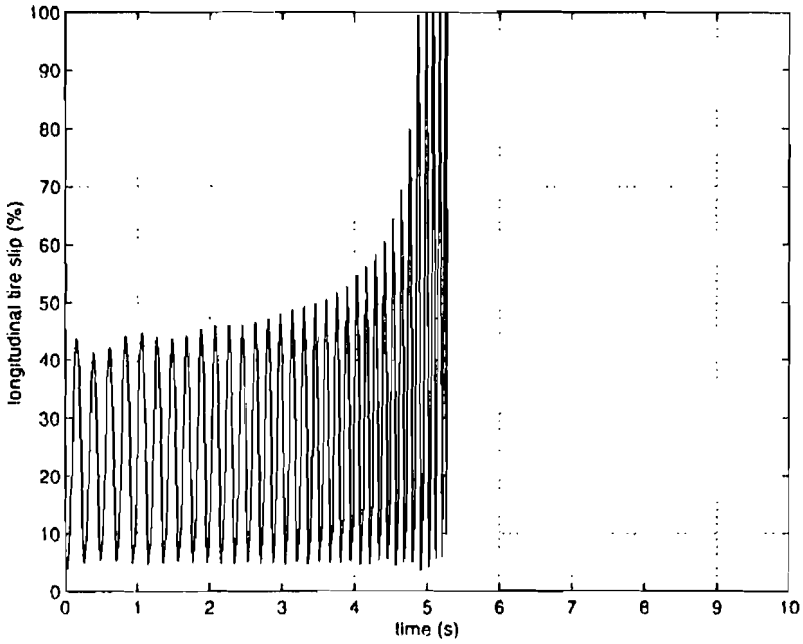

Fig. 22. (ABS) front wheel slip.

problem that has not seen much attention in the research literature [1]. The actuator is usually a hydraulic cylinder driven by a valve. The valve may be a proportional valve or a servovalve, depending on the cost restrictions. In this work, a servovalve is used as the control valve. A schematic of such an actuator system is shown in Fig. 25. The actuators are controlled by a spool valve which is, in turn, controlled by the current input to a flapper valve with a force feedback spring. The ability to generate a prescribed force from these devices is extremely nontrivial. A

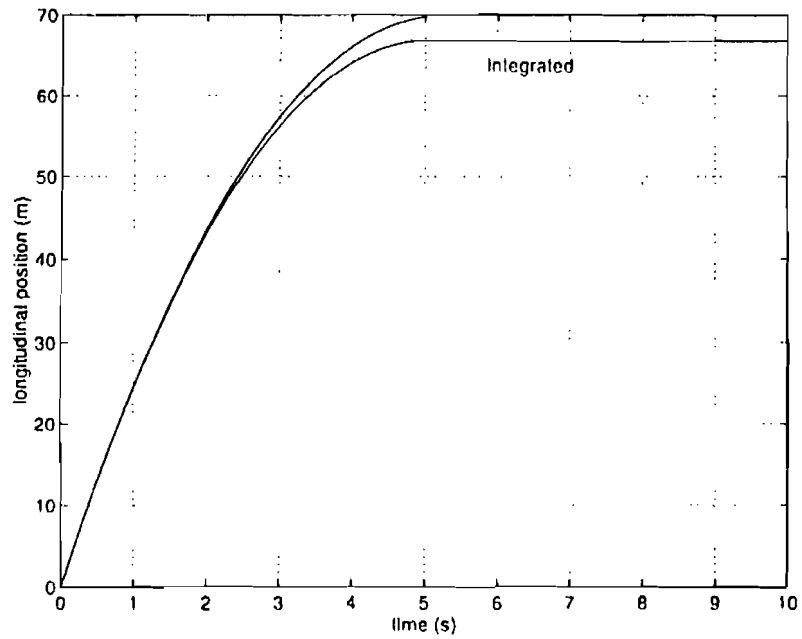

Fig. 23. (Integrated) vehicle position.

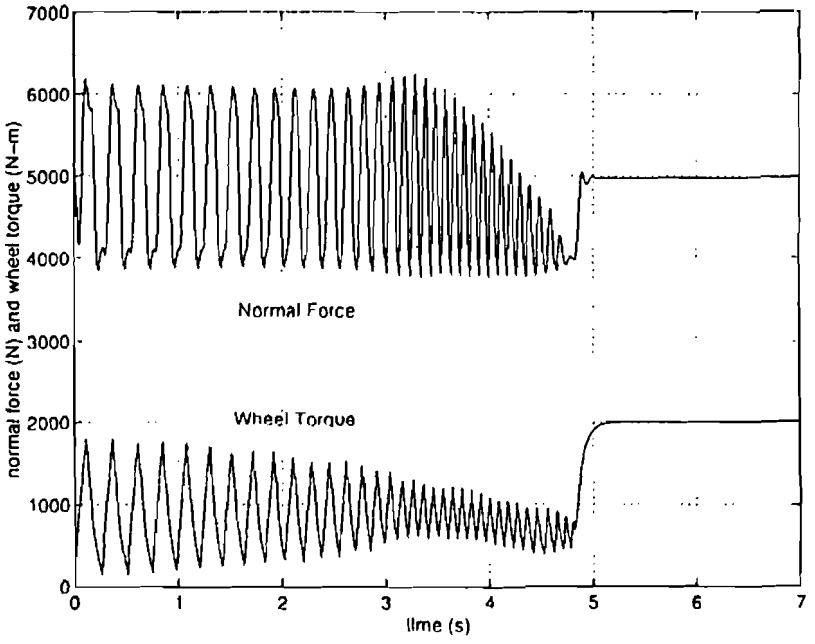

Fig. 24. Brake torque and normal force.

simple industrial PID regulator is incapable of force tracking much above one or two Hz. A more detailed view of the two stage servovalve is shown below in Fig. 26. In this analysis, the assumptions will be that the displacements of the flapper will be small, and the valve is critical center. Additionally, valve friction and flow forces will not be taken into account. This leads to the standard [13] linear representation of a two stage servovalve shown in Fig. 27. It has been experimentally verified [3] that this third order model gives a very good representation of an actual valve up to frequencies of approximately 300 Hz @ 1500psi supply pressure. The corresponding transfer function from input current to output spool displacement is

$$\frac{x_v(s)}{i(s)} = \frac{\left(\frac{K_t K_h}{K_f A_v}\right)}{s\left(\frac{s^2}{\omega_n^2} + \frac{2\zeta}{\omega_n}s + 1\right) + \left(\frac{K_t K_w}{K_f A_v}\right)} = \frac{\text{meters}}{\text{Ampere}} \tag{4.1}$$

Using typical Moog 760 series [3] servovalve parameters, the system given in

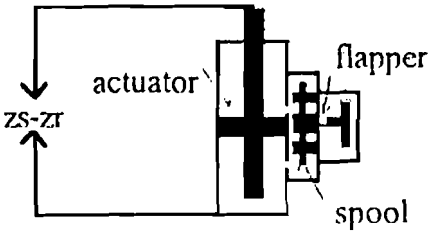

Fig. 25. Electro-hydraulic suspension actuator.

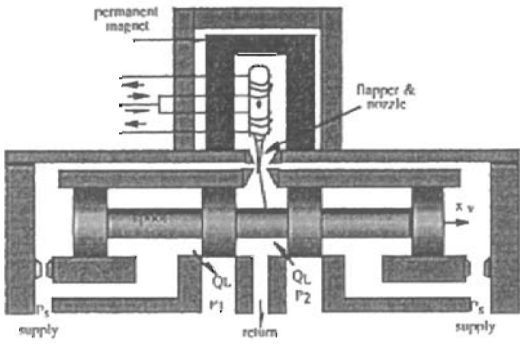

Fig. 26. Two stage hydraulic servovalve.

Equation 4.1 has three poles: two complex and one real. In the complex plane, the location of the complex poles is an order of magnitude to the left of real pole's location. Consequently, the dynamics associated with those two poles can be neglected and the servovalve acts as a first order system, with the dynamics of the real pole, up to approximately 100 Hz. The actuator dynamics given below are derived in Merritt [13] for a symmetric actuator. Defining the load pressure to be the pressure across the actuator piston, the derivative of the load pressure is given by the total load flow through the actuator divided by the fluid capacitance in the control volume:

$$\frac{V_t}{\beta_e}\dot{P}_L = -A\dot{x} - X_{tm}P_L + Q_L, \tag{4.2}$$

where V_t = total actuator volume, b_e = effective bulk modulus, A = actuator ram area, x = actuator position, and C_{tm} = coefficient of total leakage due to pressure. Using the equation for turbulent hydraulic fluid flow through an orifice, the

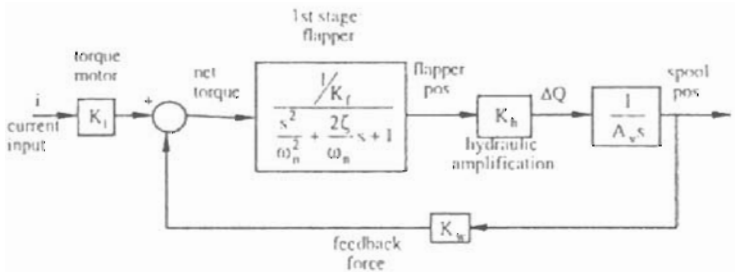

Fig. 27. Servovalve dynamics.

relationship between spool valve displacement, x_v, and the load flow Q_L, is given as:

$$Q_L = C_d w x_v \sqrt{\frac{P_s - \mathrm{sgn}(x_v)P_L}{\rho}}, \tag{4.3}$$

where P_s = supply pressure, C_d = discharge coefficient and w = spool valve area gradient. The spool area gradient for a cylindrical spool can be approximated simply as the circumference of the valve at each port. Combining Equations (4.2) and (4.3) results in the load pressure state equation

$$\begin{aligned} \dot{P}_L &= \frac{\beta_e}{V_t}\left(-A\dot{x} - C_{tm}P_L + C_d w x_v \sqrt{\frac{P_s - \mathrm{sgn}(x_v)P_L}{\rho}}\right) \\ &= -\alpha\dot{x} - \beta P_L + \gamma x_v \sqrt{P_s - \mathrm{sgn}(x_v)P_L}, \end{aligned} \tag{4.4}$$

where $\alpha := (A\beta_e/V_t)$, $\beta := (C_{tm}\beta_e/V_t)$, $\gamma := (C_d w \beta_e/V_t)\sqrt{1/\rho}$, and ρ = hydraulic fluid density.

4.2. Hydraulic System Controller Design

Define the new actuator states to be

x_{15} = Front Actuator Load Pressure $\quad x_{16}$ = Front spool valve position
x_{17} = Rear Actuator Load Pressure $\quad x_{18}$ = Rear spool valve position

Using Equation (4.1) and combining it with Equation (3.1) results in the following state equations for the front actuator subsystem:

$$\begin{aligned} \dot{x}_{15} &= -\frac{A\beta_e}{V_t}(x_2 - x_4) - \frac{C_{tm}\beta_e}{V_t}x_{15} + \frac{C_d\beta_e w}{V_t\sqrt{\rho}}x_{16}\sqrt{P_s - \mathrm{sgn}(x_{16})x_{15}} \\ &= -\alpha(x_2 - x_4) - \beta x_{15} + \left(\gamma\sqrt{P_s - \mathrm{sgn}(x_{16})x_{15}}\right)x_{16}. \\ \dot{x}_{16} &= \frac{1}{\tau}(-x_{16} + Ku_f). \end{aligned} \tag{4.5}$$

The constants τ and K are the obtained from the 1st order fit of the spool dynamics and are assumed to be the same for the front and rear actuators. The system in Equation (4.5) satisfies the Strict Feedback Form [10] for dynamic systems

$$\begin{aligned} &\dot{x}_i = f_i(x,u) && i \in [1, n-r] \\ &\dot{x}_i = f_i(x_{n-r+1} \cdots x_i) + g_i(x_{n-r+1} \cdots x_i)x_{i+1} && i \in [n-r+1, n-1] \\ &\dot{x}_n = f_n(x_{n-r+1} \cdots x_n) + g_n(x_{n-r+1} \cdots x_n)u \\ &y = h(x_{n-r+1}) \end{aligned} \tag{4.6}$$

where f, g, and h are smooth vector fields and $x \in \Re^n$, $g_i(x) \neq 0 \forall x$. 'Smooth' is meant to indicate that the functions are differentiable as needed. r is the relative degree of the system. The output of interest here is the force, or pressure, out of the actuator. It can be shown [3] that the system is nonlinear minimum phase, i.e. the system's internal states $[x_1 \cdots x_{n-r}]$ are stable. The front actuator and valve states can be rewritten in the form of Equation (4.6) for ease of subsequent analysis.

$$\dot{x}_{15} = \overbrace{-\alpha(x_2 - x_4) - \beta x_{15}}^{f_{15}} + \overbrace{\left(\gamma\sqrt{P_s - \operatorname{sgn}(x_{16})x_{15}}\right)}^{g_{15}} x_{16}$$

$$= f_{15}(x_1 \cdots x_{15}) + g_{15}(x_1 \cdots x_{15})x_{16}. \tag{4.7}$$

$$\dot{x}_{16} = \underbrace{-\frac{1}{\tau}x_{16}}_{f_{16}} + \underbrace{\frac{K}{\tau}u}_{g_{16}} = f_{16}(x_1 \cdots x_{16}) + g_{16}(x_1 \cdots x_{16})u.$$

The desired force trajectory ($F_{desired}$) can be divided by the piston area (A) to determine a desired load pressure profile ($x_{15desired}$). Define the following pressure and spool displacement errors.

$$e_{15} = x_{15} - x_{15desired} \quad e_{16} = x_{16} - x_{16desired}, \tag{4.8}$$

where the desired value of the spool displacement ($x_{16desired}$) will be determined shortly. Using the errors in Equation (4.8) define the positive definite function containing weighted squares of the errors.

$$V = \frac{\rho_{15}}{2}e_{15}^2 + \frac{\rho_{16}}{2}e_{16}^2. \tag{4.9}$$

Differentiate Equation (4.9) and substitute the expressions in Equations (4.7) and (4.8).

$$\begin{aligned} \dot{V} &= \rho_{15}e_{15}\dot{e}_{15} + \rho_{16}e_{16}\dot{e}_{16} \\ &= \rho_{15}e_{15}(f_{15} + g_{15}x_{16} - \dot{x}_{15desired}) + \rho_{16}e_{16}(f_{16} + g_{16}u - \dot{x}_{16desired}) \end{aligned} \tag{4.10}$$

Rearranging the definition of e_{16} in Equation (4.8) gives

$$x_{16} = e_{16} + x_{16desired}. \tag{4.11}$$

Substituting Equation (4.11) into (4.10) results in

$$\begin{aligned} \dot{V} = \rho_{15}e_{15}&(f_{15} + g_{15}x_{16desired} + g_{15}e_{16} - \dot{x}_{15desired}) \\ &+ \rho_{16}e_{16}(f_{16} + g_{16}u - \dot{x}_{16desired}). \end{aligned} \tag{4.12}$$

The desired value of the spool displacement can now be defined as a function of the other system states

$$x_{16desired} = \frac{1}{g_{15}}(-f_{15} + \dot{x}_{15desired} - k_{15}e_{15}), \tag{4.13}$$

resulting in

$$\dot{V} = -\rho_{15}k_{15}e_{15}^2 + \rho_{15}g_{15}e_{15}e_{16} + \rho_{16}e_{16}(f_{16} + g_{16}u - \dot{x}_{16desired}). \tag{4.14}$$

Define the actual current input to be

$$u = \frac{1}{g_{16}}\left(-f_{16} + \dot{x}_{16desired} - k_{16}e_{16} - \frac{\rho_{15}}{\rho_{16}}e_{15}g_{15}\right). \tag{4.15}$$

Substituting Equation (4.15) into Equation (4.14) gives

$$\dot{V}_1 = -\rho_{15}k_{15}e_{15}^2 - \rho_{16}k_{16}e_{16}^2 \tag{4.16}$$

which is a negative definite function of e_{15} and e_{16}. Therefore, using Lyapunov's direct method [17] the convergence of e_{15} and e_{16} to zero is guaranteed. Equations (4.13) and (4.15) give the necessary synthetic and actual inputs [1,9] for actuator force control.

$$x_{16desired} = \frac{1}{\gamma\sqrt{P_s - sgn(x_{16})x_{15}}}(\alpha(x_2 - x_4) + \beta x_{15} + \dot{x}_{15desired} - k_{15}e_{15}).$$

$$u = \frac{\tau}{K}\left[\frac{x_{16}}{\tau} + \dot{x}_{16desired} - k_{16}e_{16} - \frac{\rho_{15}}{\rho_{16}}\gamma e_{15}\sqrt{P_s - sgn(x_{16})x_{15}}\right]. \tag{4.17}$$

The ratio of ρ_{15} to ρ_{16} is chosen to normalize the contribution of each of the errors to the function V. For simplicity, ρ_{16} is chosen to be γ and ρ_{15} is adjusted. Since spool position is on the order of millimeters and the actuator load pressure is on the order of megapascals, this scaling is necessary. The expression for $\dot{x}_{16desired}$ can be determined by analytically differentiating Equation (4.13). However, in practice (Alleyne and Hedrick 1995) it is usually sufficient to numerically differentiate the computed value to determine its derivative, provided the reference trajectory is sufficiently smooth. The reference trajectory that is given by Equation

(2.15) is not smooth. Consequently, to use the nonlinear control scheme outlined above, the reference trajectory is modified as

$$F_{zdesired} = A \cdot \frac{2}{\pi} \cdot \arctan\left(\frac{(T_b - \bar{T}_b)}{\varepsilon}\right), \tag{4.18}$$

where ε can be made as small as necessary for the arctan function to approximate the sign function in a smooth, differentiable manner. The form of the controller given in Equation (4.17) points out a *key* qualitative fact that was not accounted for in previous work on electrohydraulic control. For force control of the system given in Equation (4.5), feedback of the force error (modulo the piston area) to the spool position is necessary. Additionally, for position control of the spool, the spool error should be fed back to the current input. However, *for precise actuator force control, it is necessary to also have actuator force error feedback to the spool position control algorithm.* This can be seen by the last term in the second line of Equation (4.17). This approach is significantly different from most of the "inner loop" and "outer loop" approaches to force/spool position controllers. An identical analysis for the rear electrohydraulic actuator would provide the appropriate control laws for the rear of the vehicle.

4.3. Simulations

For the simulations, the following hydraulic system parameters are added to the model:

$\alpha = 4.515e13\,N/m^5$ $\quad \beta = 1.0$ $\quad \gamma = 1.54e9\,N/m^{5/2}\,kg^{1/2}$

$\tau = 0.003$ $\quad P_s = 10342500.0\,Pa$ $\quad A = 3.35e-4\,m^2$

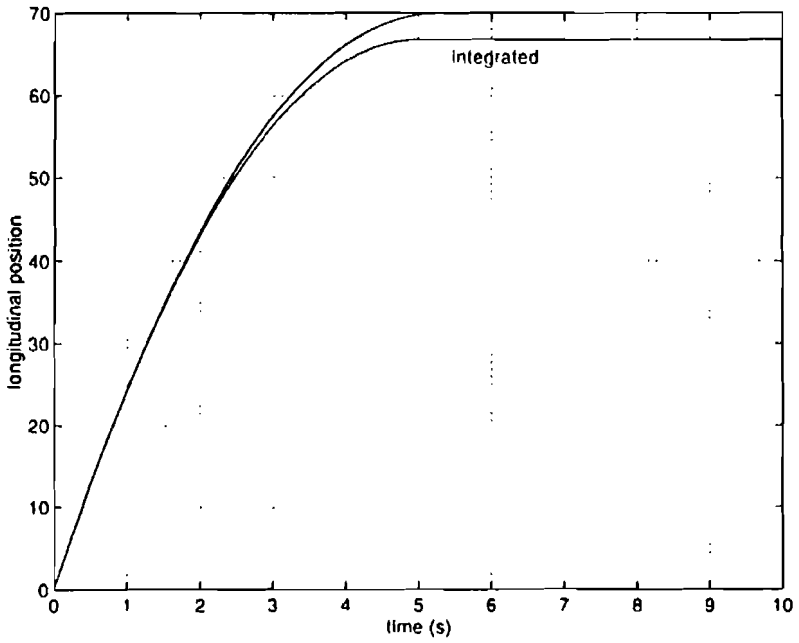

Fig. 28. (Integrated) vehicle position.

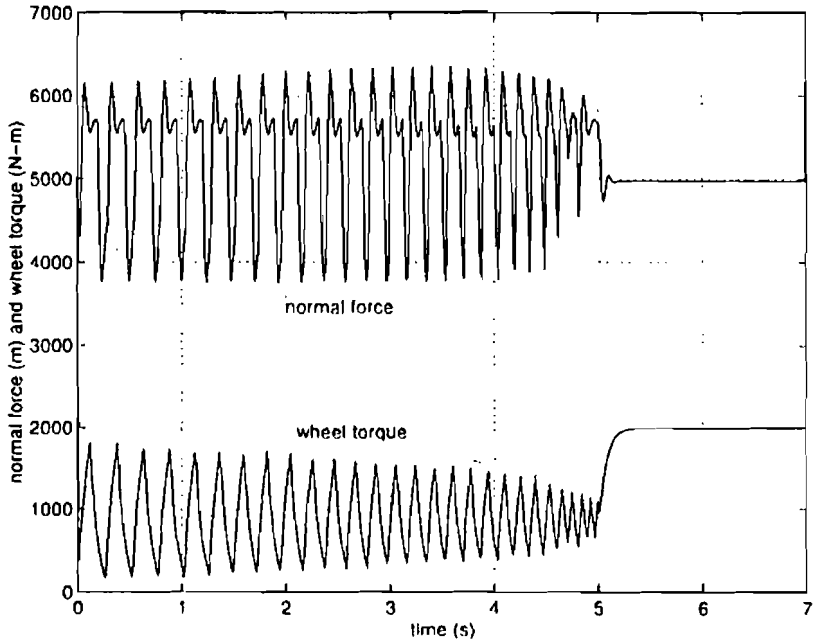

Fig. 29. Brake torque and normal force.

Identical parameters were used for the front and the rear. Fig. 28 shows the performance of the previously developed controllers for the system model augmented with actuator dynamics. The figure also shows the response of the passive system, with unsprung mass dynamics, from Section 3. Fig. 29 shows the normal force variation and the wheel torque for the front wheel. As with the previous cases, only the front wheel results are shown here. The results of the rear wheels are quite similar. As with the previous systems, the integrated control scheme of

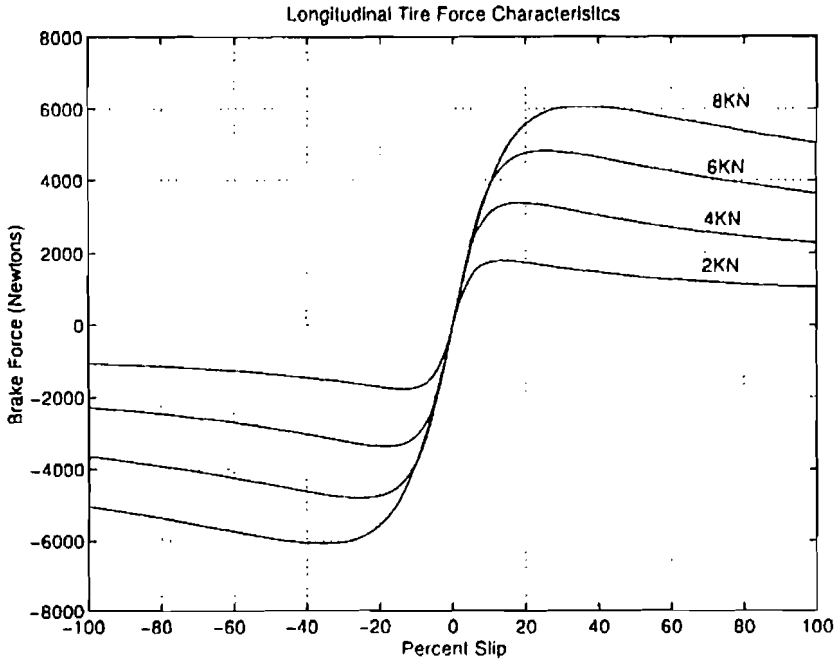

Fig. 30. Magic formula tire model.

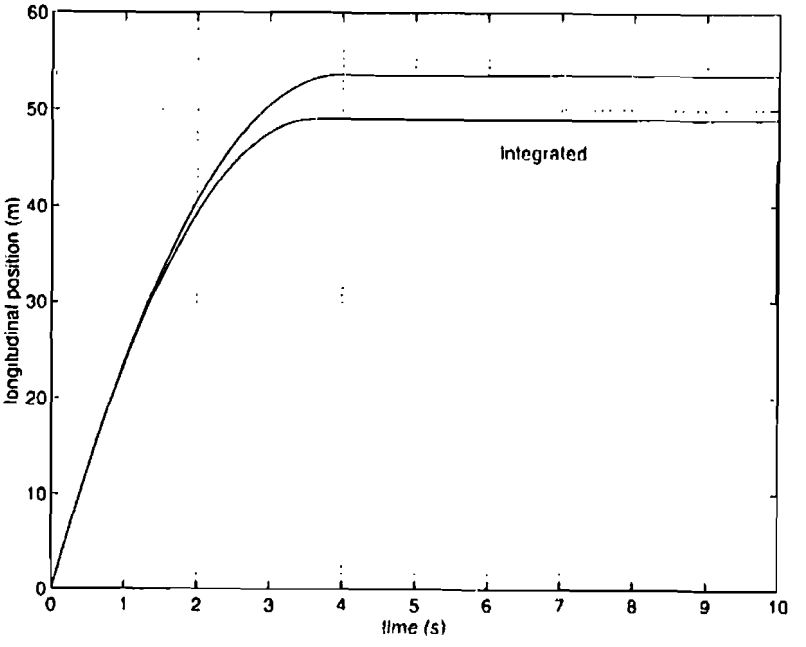

Fig. 31. (Integrated) vehicle position.

Equation (4.18) produces a significant decrease ($\sim 5\%$) in stopping distance compared to a system with only ABS.

4.4. Sensitivity to Road Condition Changes

For the road conditions given in Fig. 4, the stopping performance of the integrated approach was the same in Sections 2, 3, and 4: approximately 5% improvement over just an ABS system. As mentioned before, the effectiveness of the integrated

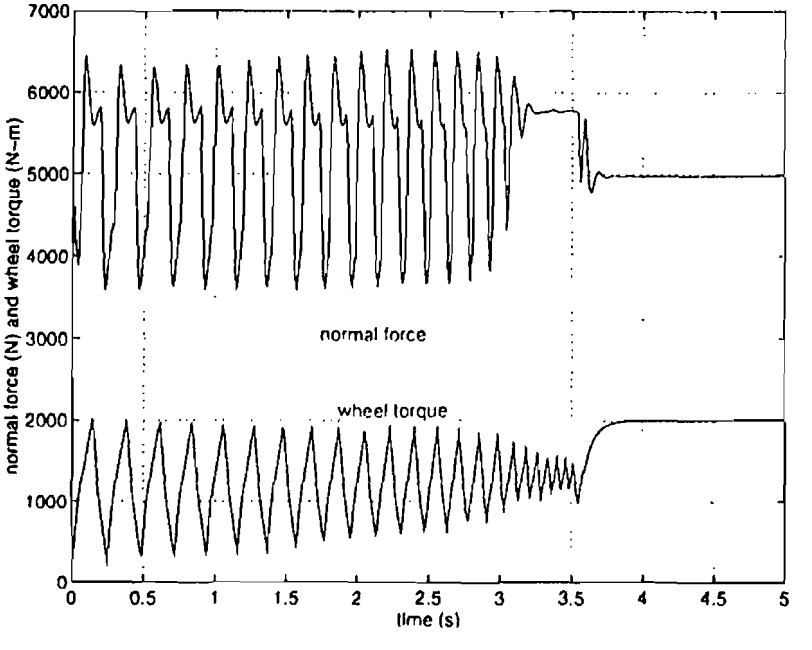

Fig. 32. Brake torque and normal force.

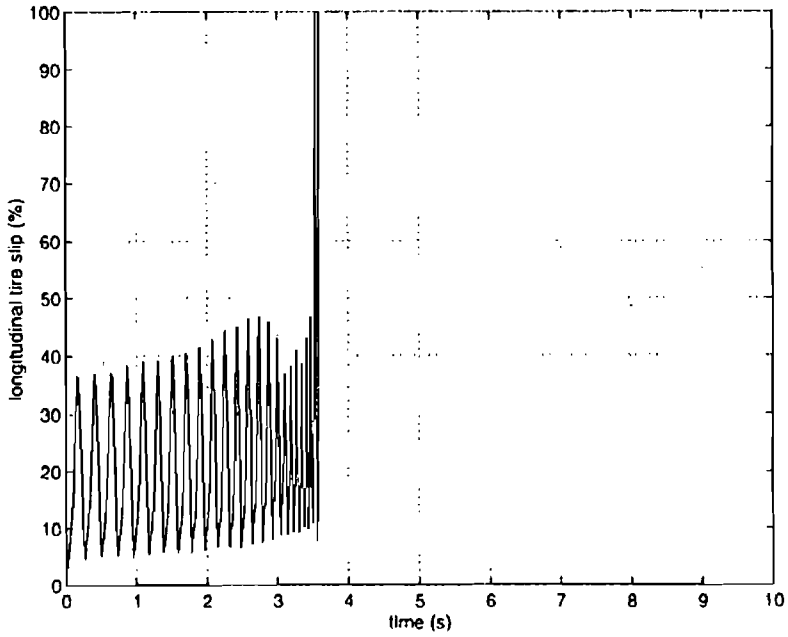

Fig. 33. Front wheel slip.

approach depends on parameters such as normal force oscillation amplitude. Another significant factor in the performance of the integrated approach is the characteristics of the tire-road interface. Changing the road surface condition will have a significant impact on the stopping performance. Fig. 30 shows the Magic Formula road condition with $a_2 = 930$ instead of 744 as before. This road configuration corresponds to a peak slip value of around 0.7 rather than the value of 0.5 that was used earlier. Fig. 31 shows the stopping distances for halfcar vehicles with just ABS and with the integrated approach. As can be seen in the figure, the integrated approach again outperforms the ABS system. However, in Fig. 31, the performance improvement is significantly larger. In the figure, the vehicle with the integrated system stops 9% shorter than the vehicle with just ABS. Fig. 32 shows the brake torque and the normal force oscillation for the front wheel. Fig. 33 shows the longitudinal percent slip as the ABS cycles on and off.

5. CONCLUSION

This paper has presented an exploratory investigation into the coordination of vehicle chassis components that has not been considered before. The components whose performances are integrated are an Active Suspension system and an ABS system. A Half Car model of a vehicle was developed along with models of an ABS system and an Active Suspension System. Two separate controllers were developed for the ABS and the Active Suspension. The controllers were then coordinated by having the desired force profile of the suspension actuator be an open loop function of the brake actuator's performance. The integrated approach was simulated along with an ABS approach. For the simulations performed, the

integrated control provided a 5 to 9 percent decrease in stopping distance on a given surface. The frequency of the suspension actuator force is above the natural frequency of the sprung mass yet below the natural frequency of the unsprung masses. Therefore, the inclusion of unsprung mass modes does not eliminate the benefit of the suspension/braking integration.

The main result of this work is to demonstrate that the integration of Active Suspensions with ABS systems is a viable chassis coordination strategy that shows significant performance benefits. Moreover, the coordination strategy can be done with existing components. The only sensor that is required for the generation of the Active Suspension force trajectory is the brake torque of the ABS. This could easily be approximated by brake pressure and obtained from a pressure sensor. The other required sensors would be no different than those that are commercially available for both ABS and Active Suspensions. For the absolute vehicle velocity measurement, some type of currently available estimation scheme would be used. While the results presented are promising, there remain several avenues for additional investigation. Chief among these is the optimization of the coordination algorithm which is the subject of ongoing research.

REFERENCES

1. Alleyne, A., and Hedrick, J. K., "Nonlinear Adaptive Control of Active Suspensions", *IEEE Transactions on Control Systems Technology*, Vol. 3, No. 1, March 1995.
2. Alleyne, A., Neuhaus, P. D. and Hedrick, J. K., "Application of Nonlinear Control Theory to Electronically Controlled Suspensions", *Vehicle System Dynamics*, Vol. 22, 1993, pp. 309–320.
3. Alleyne, A., "Nonlinear Force Control of an Electro-Hydraulic Actuator", *1996 Japan-USA Symposium on Flexible Automation*, Boston, MA, 1, 193–200, July 1996.
4. Bakker E., Pacejka, H. B., Lidner, L., "A New Tire Model with and Application in Vehicle Dynamics Studies", SAE Paper No. 890087, 1989.
5. Bobb, K., "Analysis and Identification of Dynamic Friction in a Hydraulic Actuator", University of California-SUPERB Final Report, August 1993.
6. Dreyer, A., Graber, J., Hoffman, M., Rieth, P., Schmitt, S., "Structure and Function of the Brake and Suspension Control System, BSCS", *IMechE No. C389/306 or FISITA No. 925078, Proc. of the XXIV FISITA Congress*, London, pp. 7–18, June 1992.
7. Dugoff, H., Fancher, P. S., and Segel, L., "An Analysis of Tire Traction Properties and Their Influence on Vehicle Dynamic Performance", SAE Paper No. 700377, 1970.
8. Gillespie, T. D., *Fundamentals of Vehicle Dynamics*, SAE Press, 1992.
9. Green, J. and Hedrick, J. K., "Nonlinear Speed Control for Automotive Engines", *Proceedings of the 1990 American Controls Conference*, San Diego CA, June 1990, pp. 2891–2897.
10. Kanellakopolous, I., Kokotovic, P. V., Morse, A. S., "Systematic Design of Adaptive Controllers for Feedback Linearizable Systems", *IEEE Transactions on Automatic Control*, Vol. 36, No. 11, pp. 1241–1253, November 1991.
11. Matsumoto, S., Yamaguchi, H., Inouc, H., and Yasuno, Y., "Improvement of Vehicle Dynamics Through Braking Force Distribution Control", SAE Paper 920645, ABS/Traction Control and Advanced Brake Systems, pp. 83–92, *Proc. of the 1992 SAE International Congress and Exposition*, SP-914, Detroit, MI, February, 1992.
12. Matsumoto, N., and Tomizuka, M., "Vehicle Lateral Velocity and Yaw Rate Control with Two Indpendent Control Inputs", *ASME Journal of Dynamic Systems, Measurement and Control*, Vol. 114, pp. 606–613, December 1992.
13. Merritt, H. E., *Hydraulic Control Systems*, John Wiley and Sons, 1967.

14. Miyasaki, N., Fukumoto, M., Sogo, Y., Tsukinoki, H., "Antilock Brake System (M-ABS) Based on the Friction Coefficient Between the Wheel and the Road Surface", SAE Paper 900207, ABS Traction Control and Brake Components, pp. 101–110, *Proc. of the 1990 SAE International Congress and Exposition*, Detroit, MI, February 1990.
15. Motoyama, S., Uki, H., Isoda, K., Yuasa, H., "Effect of Traction Force Distribution Control on Vehicle Dynamics", *Vehicle System Dynamics*, Volume 22, pp. 455–464, 1993.
16. Roppenecker, G., and Wallentowitz, H., "Integration of Chassis and Traction Control Systems: What is Possible – What Makes Sense – What is Under Development", *Vehicle System Dynamics*, Volume 22, pp. 283–298, 1993.
17. Slotine, J. J., and Li, W., *Applied Nonlinear Control*, Prentice Hall, 1991.
18. Tan, H. S., "Adaptive and Robust Controls with Application to Vehicle Traction Control", Ph.D. Dissertation, Department of Mechanical Engineering, University of California at Berkeley, August 1988.
19. Tseng, H. E., "A Methodology for Optimizing Semi-Active Suspensions for Automotive Applications", Ph.D. Dissertation, Department of Mechanical Engineering, University of California at Berkeley, February 1994.
20. Xia, X., and Law, E. H., "Response of Four-Wheel-Steering Vehicles to Combined Steering and Braking Inputs", DSC-Vol 13, Advanced Automotive Technologies, *Proceedings of the 1992 ASME Winter Annual Meeting*, San Francisco, CA, December 1989, pp. 107–128.